# Increasing Productivity of Ultrashort Pulsed Laser Ablation in Advance for a Combination Process with ns-laser

Andreas Brenner[1], Benedikt Bornschlegel[2], and Johannes Finger[1]

[1] *Fraunhofer Institute for Laser Technology, Steinbachstr. 15, Germany, Aachen, 52074*
[2] *Chair for Laser Technology LLT, RWTH Aachen University, Steinbachstr. 15, Germany, Aachen, 52074*
*E-mail: andreas.brenner@ilt.fraunhofer.de*

The most common way to create surface functionality in mass production are replication processes via structured mold tools. Currently used manufacturing processes for tool structuring like photochemical etching are limited in precision and in flexibility. A new and promising approach is to combine nanosecond (ns) and picosecond (ps) pulsed laser ablation sequentially to a hybrid process- similar to mechanical roughing and finishing process. However, one of the main drawbacks is the low productivity of the ps process that significantly determines the productivity of the whole combined process. To overcome the above-mentioned drawback, we investigate ultrashort pulsed laser processing using pulse bursts and varying pulse durations. By reducing the pulse duration from 10 ps to 900 fs the productivity gets doubled without any negative impact on the surface quality. Using average powers of more than 70 W an ablation rate of up to 13 $mm^3$/min is achieved. Not only productivity benefits from burst processing, but also the surface quality gets significantly improved. The roughness of a ns pre-structured surface improves from $R_a = 1.40$ µm to $R_a = 0.54$ µm.

DOI: 10.2961/jlmn.2019.01.0017

**Keywords:** burst mode, pulse duration, combination, productivity, heat accumulation, micro structuring, surface quality

## 1. Introduction

In the field of surface structuring nanosecond pulsed laser sources are established for industrial use in a wide range of applications. A crucial factor for the success of the technology is to serve a high throughput. Ultrashort laser pulses still have shown their advantages regarding highly precise ablation while minimal thermal influencing the material in diverse applications. Microstructures enable, for example, friction reduction in combustion engines or optimize the efficiency of LED-based illumination systems [1-4]. In the area of consumer products structured surfaces lead to optical and haptic functions that determine essentially the product quality. However, one of the main drawbacks is the low productivity of the ultrashort pulse laser process.

To overcome the above mentioned drawback a new and promising approach is to combine nanosecond (ns) and picosecond (ps) laser ablation to a sequentially hybrid process similar to roughing and finishing during milling [5]. The ns process is extremely determined by melt dominated ablation that leads to high ablation rates. However, melt protrusions and debris accompany the process [6-7]. In contrast, by using ultrafast laser sources new design features with higher resolution can be fabricated. Due to the mainly vaporized dominated ablation, highest precision can be achieved [8]. By a combination of these two processes their individual advantages are to be used.

Main research activities presented are different approaches for increasing productivity of ultrafast laser processing on initial grinded and in preparation of a combined process on initial ns-pretreated samples as well. The approaches consist in particular the influence of burst processing and the influence of pulse duration between 10 ps and 0.9 ps. Findings are supported by a simulation model of the temperature distributions during the laser ablation processes.

In the next section the methodology is described including the processed material, the used laser source with its burst technology and a simulation model for temperature distribution. The results are contained in section 3. At first the influence of the pulse duration while using pulse bursts is discussed ablating on an initial grinded surface. Afterwards the results of the ablation on grinded and ns-pretreated surfaces with ultrashort pulses are shown varying the number of pulses per burst and the single pulse fluence.

## 2. Method

In the following, the experimental setup and the method of the underlying investigation is described. After introducing the processed material with the two different initial surface morphologies the specialties of the used laser source are outlined. The burst technology is explained as well as the simulation model for the temperature distribution that allows for explaining the effects seen in the experimental results in section 3.2.

### 2.1 Processed material and laser source

The experimental tests are conducted on hot-working steel blanks (1.2738). The samples have two different initial quality levels. One sample was grinded until a surface roughness of $R_a = 0.35 \pm 0.02$ µm is reached. Another sample was treated with ns laser pulses resulting in a surface roughness of $R_a = 1.40 \pm 0.26$ µm (cf. **Fig. 1**). The experimental tests are carried out identically on both of these samples. Squared cavities with a dimension of 6 x 6 $mm^2$ are produced applying a bidirectional scan strategy with an angle of 0° and 90°. In all results presented here, the number of layers (N) is kept constant at 50 scans per cavity.

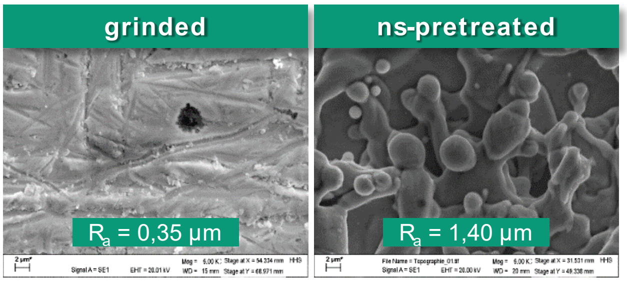


**Fig. 1** SEM images of sample surfaces. Grinded sample with an initial average surface roughness of $R_a = 0.35 \pm 0.02$ µm. Ns-pretreated sample with an initial average surface roughness of $R_a = 1.40 \pm 0.26$ µm.

The experimental setup consists of a high power ultrafast laser source from Amphos with a maximum average power of $P_{av}$ = 145 W and an adjustable pulse duration $\tau$ between 10 ps and 900 fs. The amplifier is based on the InnoSlab concept, a design of the master oscillator power amplifier (MOPA) that was developed at Fraunhofer ILT. The emitted laser radiation has a wavelength of 1030 nm (Yb:YAG) and an adjustable pulse repetition rate $\nu_{rep}$ between 250 kHz and 4 MHz. The seeder frequency $f_{seed}$ is 37.86 MHz. The laser beam is moved by a galvanometer scanner (Arges Rhino 16) and focused on the tool steel surface with a focal length of f = 163 mm. The focus diameter ($1/e^2$) is about $2w_0$ = 35 µm (measured with a camera based beam profiler) at a theoretical Rayleigh length of about $z_R$ = 940 µm. To obtain reproducible and correct average overlapping pulses the feed per pulse (i.e. scan speed $v_f$) and the line distance (LD) is fixed at 8 µm.

## 2.2 Burst technology

Besides the adjustable pulse duration the high power ultrafast laser source offers the so called burst technology. These promises to increase productivity in ultrafast laser ablation. The master oscillator creates pulses with low energy and a high repetition frequency of (about) 37.86 MHz. An electro-optic pulse picker (EOM) selects one pulse out of e.g. 77 pulses so that a repetition frequency of approx. 500 kHz is created. The pulse picker can also select several pulses instead of one, so that these pulses packaged in a group are called "bursts".

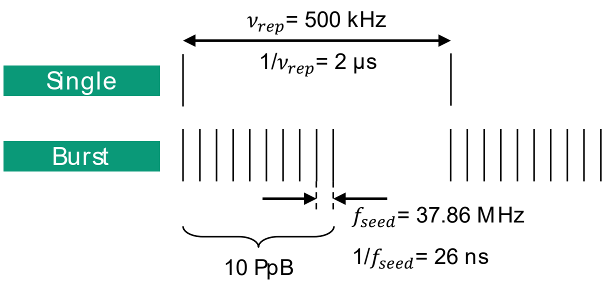


**Fig. 2** Illustration of pulse to pulse frequencies and corresponding time periods for single pulse and burst technology.

The time period between two pulses in a burst amounts only 26 ns. In comparison to that, the time between two single pulses is about several µs (cf. **Fig. 2**). The pulse picker allows to apply a number of pulses between 1 and 10 to a burst. In the following this parameter "Pulse per Burst" will be abbreviated with PpB. Finally, these bursts are amplified in the amplifier, while the energy is distributed equally over the pulses. So for example an energy of about 500 µJ for a single pulse will be split up into a group of ten pulses with about 50 µJ per pulse. This kind of Amphos laser source provides a maximum average power of 145 W while generating a maximum pulse energy of 500 µJ at a repetition frequency of 250 kHz.

## 2.3 Simulation model temperature distribution

Even for ultrashort laser processing a certain amount of the laser pulse energy incident on the sample surface does not contribute to the ablation process and is deposited as residual heat in the material. For steel 1.4301 Bauer et al. determined by calorimetric measurement that up to $\eta_{res}$ = 40 % of the laser pulse energy remains as heat in the solid workpiece [9]. This residual energy can accumulate and lead to thermal effects within the processed material.

For burst processing, when multi pulses impinge the surface with a frequency in MHz regime, the small amount of residual heat that is introduced into the material by a single pulse may not be completely dissipated into the sample by heat conduction before the next pulse is applied after a view nanoseconds. As a result to that, the following pulse (e.g. in the same burst) hits a locally preheated workpiece and heats it up to an even higher temperature [10].

The coefficient $\eta_{res}$ is extremely determined by the material properties (e.g. optical properties, energy penetration depth, ablation threshold) and the applied laser processing parameter. Vorobyev et al. determined at first residual heat coefficients for several materials (Cu, Mg, Au, Si, Al) depending on the applied single pulse fluence of ns and fs laser ablation using calorimetric technique [11-12]. Finger set as a result of theoretical calculations and observed experimental results the remaining heat coefficient for Inconel 718 in the range between 30 % and 40 % [13]. In the following simulation the residual heat coefficient $\eta_{res}$ for hot-working steel 1.2738 is set to 35 % that agrees well with the literature.

Assuming the spatial laser intensity distribution follows a Gaussian beam and represents a surface heat source the temperature raise at $t = 0$ at the location ($x_0$, $y_0$, 0) can be calculated by [9]

$$T^{s.p.}_{x_0,y_0}(x,y,z,t) = \frac{2\eta_{res} \cdot E_p}{\pi\rho c \cdot \sqrt{\pi\kappa t}(8at + w_0^2)} \cdot \exp\left[\frac{(x-x_0)^2 + (y-y_0)^2}{4at} \cdot \left(\frac{w_0^2}{8at + w_0^2} - 1\right)\right] \cdot \exp\left[-\frac{z^2}{4at}\right] \quad (1)$$

with laser pulse energy $E_p$, density $\rho$, specific heat capacity $c$ and thermal diffusivity $a$.

For a burst with $n$ pulses and a scan speed $v_f$ along the x-axes the temperature distribution follows [14]

$$T^{b}_{x_0,0}(x,y,z,t) = \sum_{i=0}^{n-1} T^{s.p.}_{x_i,0}(x,y,z,t_i) \quad (2)$$

The following Table 1 gives an overview about the material properties of hot-working steel 1.2738 that are used for the simulation model.

**Table 1** Material properties of hot-working steel 1.2738

| Material properties | 1.2738 |
|---|---|
| Density $\rho$ | 7800 kg/m³ |
| Heat capacity $c$ | 460 J/kg/K |
| Thermal diffusivity $a$ ($\times 10^{-6}$) | 9.615 m²/s |
| Residual heat factor $\eta_{res}$ | 0.35 |

In **Fig. 3** a simulation of the temperature distribution is illustrated. A residual heat factor of 35 % is assumed. Besides the material properties the temperature distribution is strongly determined by the laser process parameters and the spatial and temporal displacement. The shown simulation result is calculated with a spot diameter $2w_0$ = 35 µm, a laser fluence $F_0$ = 3 J/cm², a scanning speed $v_f$ = 4 m/s, a repetition frequency $\nu_{rep}$ = 500 kHz and 10 pules within a burst.

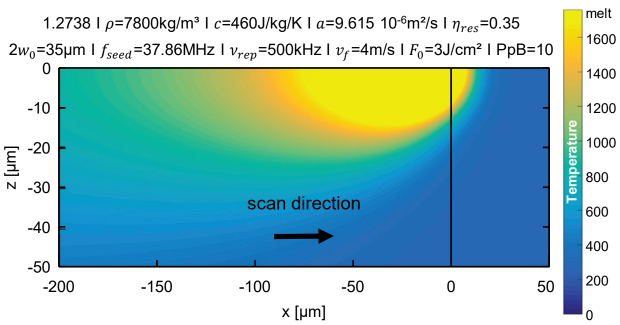


**Fig. 3** Temperature distribution after absorption of a series of pulse bursts containing 10 pulses each. The next pulse burst impinge a preheated and molten surface at position $x = 0$.

The temperature distribution shows the situation at a time when the next group of 10 pulses will impinge on the surface at position $x = 0$. The sample is in its molten state at this time due to heat accumulation as a result of previous pulse bursts that hit the surface with $\Delta x$ = 8 µm. Taking the melting enthalpy into account, the melt temperature for 1.2738 is set to 1759.15 K. The simulation helps to understand how the surface looks like while interacting with ultrashort laser pulses (cf. section 3.2).

## 3. Results and Discussion

To analyze the produced cavities a laser scanning microscope (Keyence VK 9700) is used. Target figures for examination are the surface roughness ($R_a$ and $R_z$) and the ablation depth ($\Delta z$) that is used to calculate the ablation rate dV/dt and the power specific volume ablation rate dV/dt/$P_{av}$ for measuring the efficiency of the ablation process. The surface roughness was measured by using a magnification lens of 50x together with a cut-off length of 0.08 mm. In order to obtain a representative value for the surface roughness it was calculated by the average of 60 line roughness that cover the surface.

At first, the influence of the pulse duration on the ablation efficiency and on the surface roughness is discussed while ablating on an initial grinded surface. In the following the results of the ultrashort pulsed laser ablation on an initial grinded as well as on an initial ns-pretreated surface are shown. Here the effect of heat accumulation is presented by varying the number of pulses per burst and the incident single pulse fluence. By comparing the simulation model of the temperature distribution with the surface morphology, the results can be explained as a consequence of heat accumulation. Also a correlation between the measured surface roughness and simulated melt pool depth can be found. Furthermore, the achieved volume ablation rates are presented.

### 3.1 Influence of the pulse duration and number of pulses per burst

#### 3.1.1 Ablation efficiency

The dependence of the ablation efficiency (ablated volume per time and average power) on the pulse duration for grinded hot working steel 1.2738 is shown in **Fig. 4**. The experimental data presented are for different pulse durations of 0.9, 4, 7 and 10 ps. Parameters like single pulse peak fluence, pulse repetition frequency, scan speed, line distance or number of layers are kept constant. Only the number of pulses per burst are varied – 1, 2, 4, 6, 8 and 10. As a result of burst processing the ablation efficiency drops in comparison with single pulse ablation for all pulse durations between 0.9 ps and 10 ps. Shielding effects of ablated particles prevent an energy transfer to the work piece so that in consequence less energy contributes to the ablation process. However, the ablation efficiency for 4 and 6 pulses per burst is less than for 8 and 10 pulses that strikes the theory mentioned above. A possible explanation can be that heat accumulation overcompensate the shielding at this point.

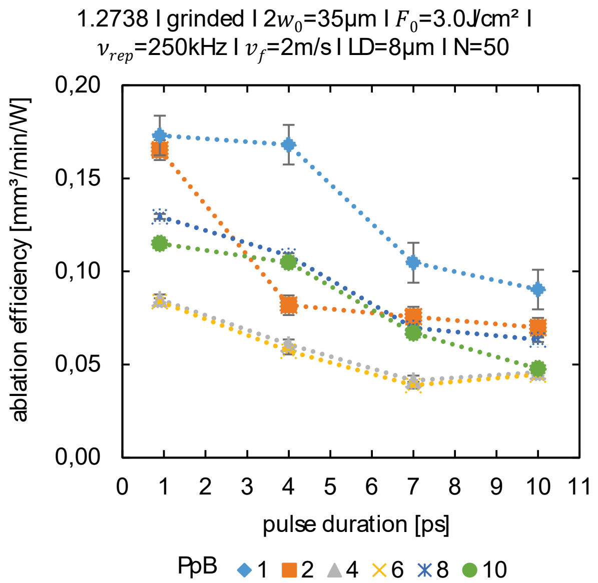


**Fig. 4** Measured ablation efficiency depending on the pulse duration for different numbers of pulses per burst (PpB) – 1, 2, 4, 6, 8 and 10.

Overall, the ablation efficiency increases for every burst configuration by reducing the pulse duration. A reason can be found in the change of the effective penetration depth $\delta_{eff}$ by reducing the pulse duration. The following equation illustrates the influence of the effective penetration depth and supports as a theoretical explanation. The ablated volume for a pulsed Gaussian beam with a spot radius $w_0^2$ depends essentially on the incident ($F$) and threshold fluences ($F_{th}$) and on the effectively penetration depth ($\delta_{eff}$) [13, 15]:

$$\Delta V = \frac{1}{4}\pi \cdot w_0^2 \cdot \delta_{eff} \cdot \ln^2\left(\frac{F}{F_{th}}\right) \qquad (3)$$

While keeping the incident fluence ($F$) constant and without almost no change in threshold fluence ($F_{th}$) while changing pulse duration [16] the result for higher ablation efficiencies has its reason in an increased penetration depth ($\delta_{eff}$) for decreased pulse durations [17]. For single pulse ablation the effect is already observed for several materials (steel, copper, Inconel) [13 and 17-19]. This examination shows that also for burst processing the ablation efficiency increases by decreasing the pulse duration. On the one hand side burst processing reduces the nominal ablation efficiency due to pulse-to-pulse interaction and correlated shielding effects (cf. ablation with high repetition frequencies in [13]). On the other hand side shorter pulse durations in the range of 1 ps lead to an increase of ablation efficiency also for pulse burst processing having a look at the results shown in **Fig. 5**.

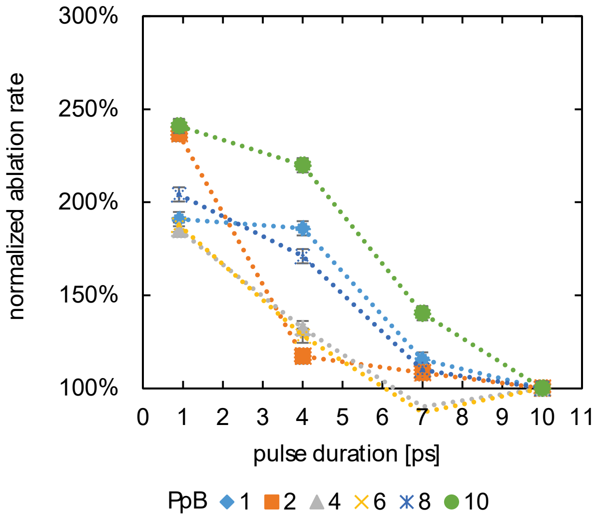


**Fig. 5** Normalized ablation efficiency depending on the pulse duration. The measured data are each normalized to the efficiency data at 10 ps.

The nominal measured ablation efficiencies for 1 PpB and 2 PpB are the highest for all pulse durations with exception at 4 ps. Parameters with 4 PpB and 6 PpB achieve the lowest efficiency for all pulse durations, while 8 PpB and 10 PpB are in between. Due to the high seed laser frequency of 37.86 MHz the time between two pulses in a burst amounts only 26 ns. This short period of time leads to pulse-to-pulse interaction so that only a part of the pulse energy is available for the ablation process. The rise of the ablation efficiency as a result of reducing the pulse duration from 10 ps to 0.9 ps is between 85 % for 4 PpB and 141 % for 10 PpB. The average rise of ablation efficiency is about 0.034 mm³/min/W for reducing the pulse duration by one picosecond.

For better identification of the influence of the pulse duration on pulse-to-pulse interaction in **Fig. 5** the ablation efficiency is normalized to the measured efficiency at 10 ps. It is shown that for 10 PpB the relative rise of ablation efficiency is stronger than for single pulse (1 PpB) ablation by reducing pulse duration from 10 ps to 0.9 ps. As a result of higher ablation efficiency for shorter pulse durations one would expect that particle shielding is more pronounced for the use of shorter pulses. However, the results show the opposite effect. A decrease of pulse duration not only leads to higher ablation efficiencies but also to less pulse-to-pulse interaction and less shielding for burst processing. Similar results are observed by Finger with high single pulse repetition frequency up to 7.1 MHz [13]. One possible explanation for this behavior is that the ablation plume and particles propagate faster for applying shorter pulse durations. Therefore, the shielding of subsequent pulses within a burst is less pronounced because the plume is less dense when the next pulse arrives. Another reason could be that the size distribution of the ablated particles differs for the use of shorter pulse durations. In consequence, other scattering mechanisms determine the pulse to pulse interactions when applying shorter pulses.

### 3.1.2 Surface roughness

As shown in **Fig. 6** there is no significant influence of the pulse duration to the surface roughness. If there is a weak correlation then the surface roughness tends to become better by reducing the pulse duration whereby the measured data are within the standard deviation.

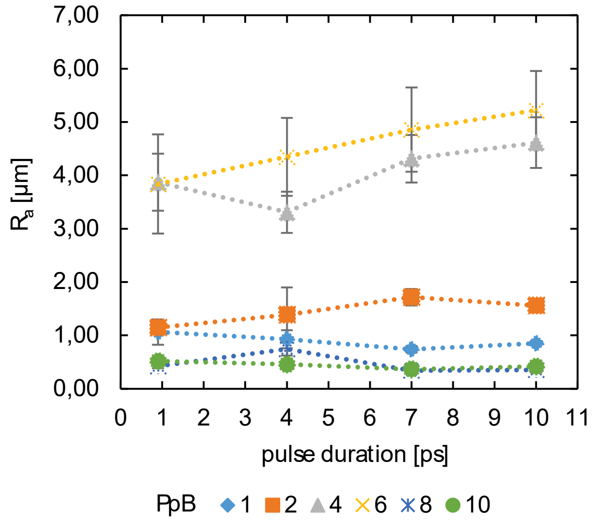


**Fig. 6** Measured surface roughness $R_a$ depending on the pulse duration for different numbers of pulses per burst (PpB) – 1, 2, 4, 6, 8 and 10.

These results show that laser ablation processing of metals like 1.2738 with ultrashort laser pulses in the range of 1 ps or lower promises advantages in efficiency that lead to increased productivity by a factor of approx. 2 in the end. In the following examination the experiments are only processed at this working point with a pulse duration of 900 fs.

### 3.2 Influence of number of pulses per burst and fluence on different initial pretreated surfaces

#### 3.2.1 Surface morphology and surface roughness

In the following, the influence of pulse bursts on the surface quality is examined while varying the single pulse energy. Pulse bursts consisting of one pulses to ten pulses (1 PpB to 10 PpB) are applied. The single pulse peak fluence ($F_0$) is varied between 0.8 J/cm² and 3.0 J/cm².

Thus, a pulse burst with ten pulses (10 PpB) possess energy ten times higher than a pulse burst with only one pulse (1 PpB) that has to be considered. The pulse duration is kept constant for productivity reasons at 0.9 ps (cf. section 3.1). Pulse repetition frequency, scan speed, line distance and number of layers are kept constant for comparison purposes.

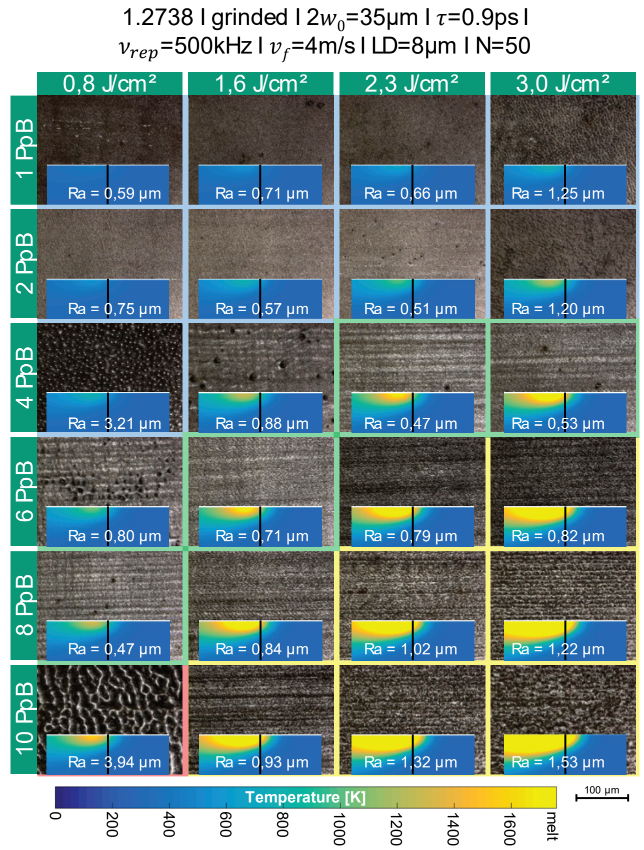


**Fig. 7** Development of the surface morphology on the initial grinded sample in dependence of the applied number of pulses per burst (PpB) and single pulse fluence. A corresponding simulation of the temperature distribution illustrates the effect of heat accumulation. 3 ablation regimes can be identified (blue, green, yellow)

In **Fig. 7** the effect of the number of pulses per burst and the corresponding applied single pulse fluence within the burst on the initial grinded surface is illustrated. In **Fig. 8** the effect on the initial ns-pretreated surface is shown. On the one hand side the amount of heat accumulation can be controlled by the number of pulses per burst. On the other hand side the single pulse fluence determines the effect of heat accumulation at the surface as well [cf. 14]. A simulation of the temperature distribution following the model described in section 2.3 is assigned to each processing parameter. The development of heat accumulation depending on the number of pulses per burst and on the fluence is supported and visualized by the simulation model.

Applying one or two pulses per burst the ablation process is accompanied without heat accumulation regardless of the used fluence. The ablation process here is determined by ultrashort pulsed specific vaporization. Here the surface roughness depends obviously on the initial surface. While applying 1 or 2 PpB on the grinded surface ($R_a$ = 0.35 µm) the obtained surface roughness varies between 0.51 and 1.25 µm. Doing the same on the ns-pretreated surface ($R_a$ = 1.40 µm) the processed surface shows a roughness between 1.11 and 1.59 µm.

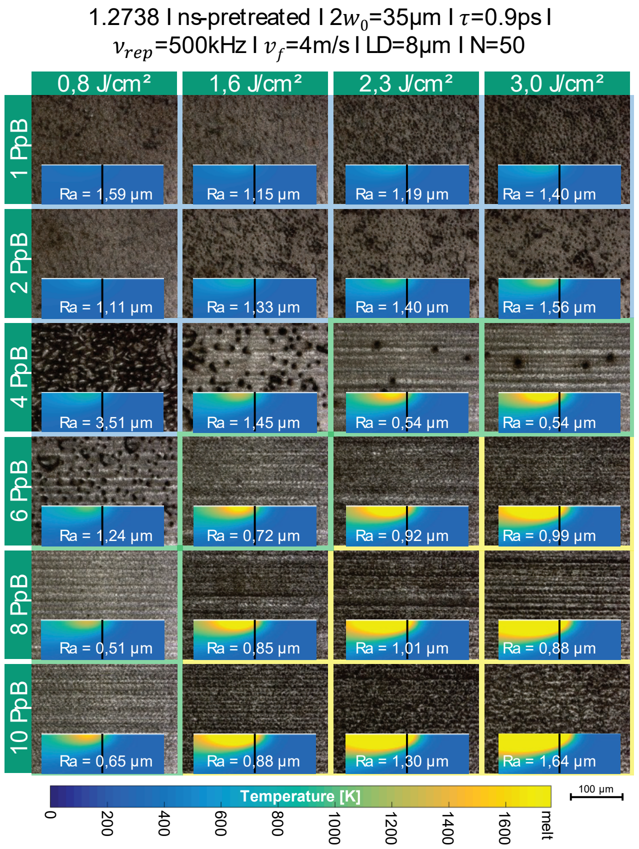


**Fig. 8** Development of the surface morphology on the initial ns-pretreated sample in dependence of the applied number of pulses per burst (PpB) and single pulse fluence. A corresponding simulation of the temperature distribution illustrates the effect of heat accumulation. 3 ablation regimes could be identified (blue, green, yellow)

Focusing on the heat development while processing with 8 or 10 PpB the simulation model offers that independent of the fluence a melt pool is formed. As a result the development of the surface morphology tends to get rougher while increasing the fluence (with an exception for grinded surface, 10 PpB, 0.8 J/cm²). Due to the heat accumulation the next pulses impinges on a preheated and molten surface that causes an inconsistent consolidation. Here the difference regarding the initial surface morphology is not important any more. As a result of the formed melt pool the ns-pretreated surface is smoothed due to the surface tension of the melt. Thus, the resulting surface roughness varies in the same range regardless of the initial surface roughness (grinded sample: 0.47 µm to 1.53 µm; ns-pretreated sample: 0.51 µm to 1.64 µm). The resulting surface roughness seems to be determined only by the laser processing parameter. One exception is the surface applying 10 PpB with a fluence of 0.8 J/cm². While receiving a smoothed surface processing on the ns-pretreated sample ($R_a$ = 0.65 µm) the surface morphology on the grinded sample is dominated by fused craters ($R_a$ = 3.94 µm). A reason could not be fund yet and further investigations are necessary.

Processing with 6 PpB and a low fluence of 0.8 J/cm² the surface gets covered by holes that occur more on the ns-pretreated surface ($R_a$ = 1.24 µm) than on the grinded surface ($R_a$ = 0.80 µm). Regarding the simulation model for this parameter combination the heat accumulation is not as pronounced that a melt pool is formed. By increasing the fluence to 1.6 J/cm² the melt ensures a better surface quality (ns-pretreated: 0.72 µm, grinded: 0.71 µm). A further increase of the fluence leads to a rougher surface but still better than processing with 8 or 10 PpB.

According to processing 6 PpB the fluence is also strongly determining the surface quality while applying 4 PpB. Using 0.8 J/cm² the grinded as well as the ns-pretreated surface is littered with tiny peaks that cause a very rough surface (ns-pretreated: 3.51 µm, grinded: 3.21 µm). Increasing the fluence to 1.6 J/cm² ensures the peaks to disappear but induces holes similar to the parameter combination 6 PpB and 0.8 J/cm². The surface is smoothed by further increasing the fluence and heat accumulation that leads to the best surface quality at a fluence of 2.3 J/cm². Here a surface roughness of 0.47 µm for the grinded surface and 0.54 µm for the ns-pretreated surface is obtained. Nevertheless a few holes are also created on this surface.

To sum up, the observed ablation process could be divided into three different regimes. The first regime (highlighted in blue) describes the ablation without a developed melt pool. Heat accumulation does not affect the result. The surface roughness is extremely determined by the initial existing surface like Neuenschwander saw on different mechanical pretreated surfaces [20]. The ablation process is dominated by vaporization.

In the second regime (highlighted in green) a melt pool is build, but the following pulse burst impinges on an already consolidated surfaces. The already existing melt pool ensures that roughness peaks are smoothed due to the surface tension of the melt. As a result initial rough surfaces can be smoothed and ablated with good quality at the same time. This ablation regime is very interesting and a specific characteristic for ultrashort pulsed burst ablation. It promises moderate ablation rates and best surface qualities regardless of the initial surface quality due to melt-induced surface tension.

In the third regime (highlighted in yellow) a melt pool is build. The ablation process is significantly determined by heat accumulation that influences the morphology of the surface structure. According to the simulated temperature distributions, the next pulse burst is applied on molten material. That leads to rougher surfaces by melt ejections. The ablation process is comparable to the melt dominated ablation with longer nanosecond pulses.

### 3.2.2 Correlation between measured surface roughness and simulated melt pool depth

A consideration of a possible correlation between the simulated melt pool depth and the obtained surface roughness reveals that, from a certain point onwards, the melt pool depth is equal to the averaged roughness depth $R_z$. **Fig. 9** and **Fig. 10** show the averaged roughness depth $R_z$ as a function of the melt pool depth, simulated by the model described in section 2.3.

The averaged roughness depth $R_z$ is the average of individual roughness depths of five consecutive individual measuring paths in the roughness profile. In each measuring segment, the extreme values are added to a range and divided by the number of measuring segments.

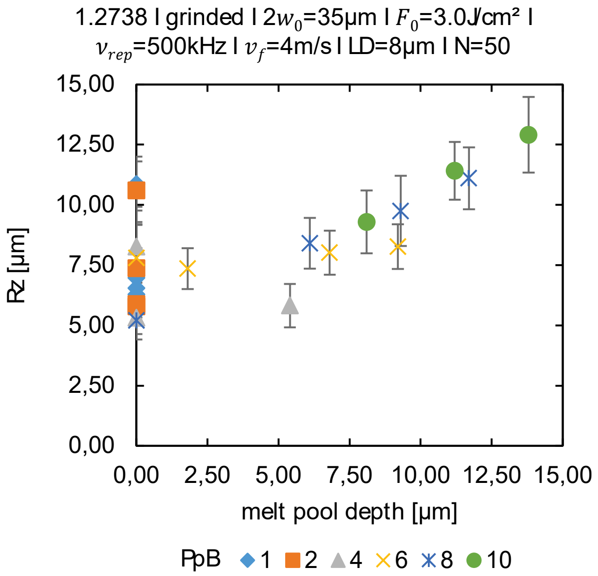


**Fig. 9** Averaged roughness depth $R_z$ as a function of the simulated melt pool depth for different numbers of pulses per burst applied at a grinded sample.

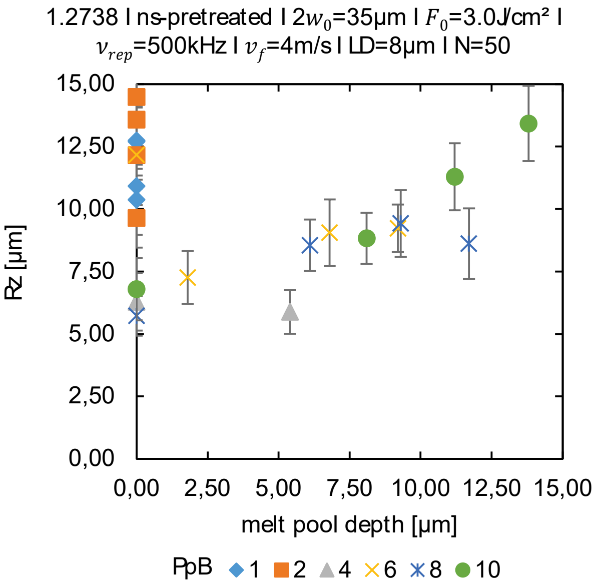


**Fig. 10** Averaged roughness depth $R_z$ as a function of the simulated melt pool depth for different numbers of pulses per burst applied at a grinded sample.

This correlation phenomena could be observed processing on the grinded surface (cf. **Fig. 9**) as well as on the ns-pretreated surface (**Fig. 10**). As soon as the process is in the third regime (highlighted in yellow), a melt pool is formed that obviously determines significantly the surface roughness. A melt pool depth of 5.40 µm for 4 PpB and 3 J/cm² leads to a roughness depth of 5.88 ± 0.88 µm. As a result of increasing either the number of pulses per burst or the fluence, heat accumulation causes a more pronounced melt pool. 10 PpB and a fluence of 3 J/cm² finally lead to a melt pool depth of 13.80 µm while the measured roughness depth is 13.42 ± 1.51 µm. If the process parameters do not form a melt pool, the surface roughness cannot be predicted with this explanation model.

### 3.2.3 Volume ablation rate

In **Fig. 11** and in **Fig. 12** the corresponding ablation rates depending on the applied number of pulses per burst and single pulse fluence are illustrated for the initial grinded and ns-pretreated samples. By increasing the pulses per burst and the fluence respectively the ablation rate can be improved significantly.

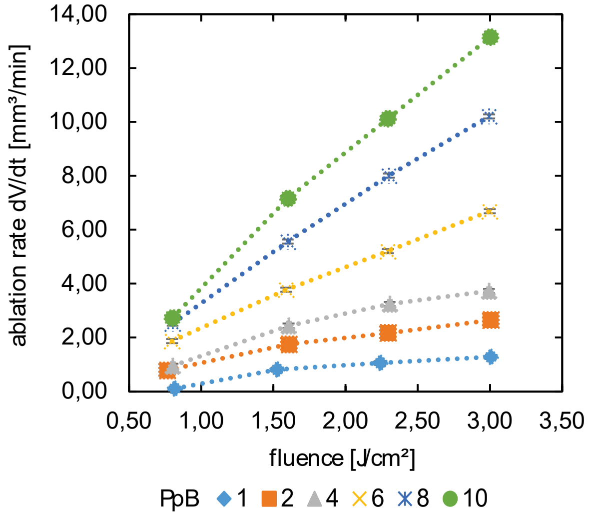


**Fig. 11** Dependence of the applied number of pulses per burst and the single pulse fluence on the ablation rate on an initial grinded surface. The maximum accomplished ablation rate is 13.14 mm³/min.

While single pulse processing with 0.8 J/cm² achieves an ablation rate of 0.11 mm³/min, 10 PpB reach 2.73 mm³/min for the grinded surface. For single pulses with a fluence of 3 J/cm² a maximum ablation rate of 1.28 mm³/min is measured. Applying the same single pulse fluence to 10 pulses within a burst a maximum ablation rate of 13.14 mm³/min is achieved (cf. **Fig. 11**). This value is one order of magnitude higher compared to ablation rates achieved with single pulse processing. However, the applied energy is also one order of magnitude higher for this comparison (cf. section 2.2). Nevertheless, only the burst technology enables to transfer such an amount of energy to the surface while achieving appropriate surface qualities (cf. **Fig. 7**) using galvanometer scanners. The ablation rate is calculated with an ideal duty cycle of 100 %.

Similar results were achieved for ablation on the ns-pretreated surface (cf. **Fig. 12**). Single pulse processing with 0.8 J/cm² leads to an ablation rate of 0.37 mm³/min, while 10 PpB accomplish 3.67 mm³/min. Applying a fluence of 3 J/cm² an ablation rate for single pulses of 1.19 mm³/min respectively for 10 PpB of 13.63 mm³/min is measured. Finally an average power of approximately 72 W is used to realize such an ablation rate with ultrashort laser pulses. The related surface qualities are shown in **Fig. 7** and in **Fig. 8**.

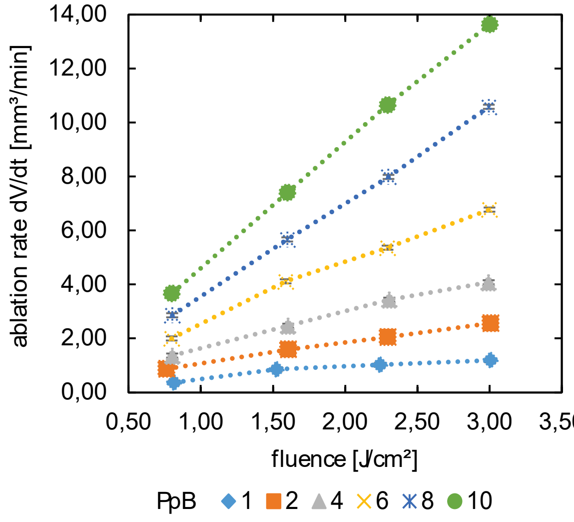


**Fig. 12** Dependence of the applied number of pulses per burst and the single pulse fluence on the ablation rate on initial ns-pretreated surface. The maximum accomplished ablation rate is 13.63 mm³/min.

## 4. Conclusions

For a combination process using high productive nanosecond and very precise picosecond laser pulses the bottle neck for productivity is still the ultrashort processing. Thus, investigation of the pulse duration dependence and burst processing on ultrashort pulsed laser ablation of 1.2738 hot-working steel to increase productivity are presented. Using high power InnoSlab picosecond lasers in master oscillator power amplifier (MOPA) design, it is possible to generate pulse bursts with a selectable number of pulses per burst. In addition to that, a new designed compressor enables an adjustable pulse duration between 10 ps and 0.9 ps utilizing the same laser active medium.

The reduction of the pulse duration leads to a significant improvement of productivity between 185 % and 241 % depending on the number of pulses per burst applied. Besides the known increase of the ablation efficiency for using shorter pulse durations, a decrease of shielding effects for the use of pulse bursts is observed. A negative impact on the surface quality quantified by the surface roughness could not been identified. Thus, a pulse duration of 900 fs is a preferable working point for micro ablation of hot-working steel 1.2738. Similar results show the investigation of Russ et al. [21] who compared three lasers with pulse durations of 400 fs, 900 fs and 6 ps and confirmed that the ablated volume for 400 fs in neither case could exceed the 900 fs level. Pointing out that the energy penetration depth

$\delta_{eff}$ at 400 fs and 900 fs seems to be quite similar, they measure a difference in the threshold fluence $F_{th}$. Following equation 3 this leads to the effect, that even for a similar penetration depth at 400 fs the ablated volume per pulse is lower than at 900 fs. They assume that nonlinear effects could cause a distortion of the beam profile that led to an irregular ablation. However, Jaeggi et al. measured a rise in the average power specific volume ablation rate by decreasing the pulse duration to 350 fs [19]. Finally further investigations are necessary to make a decision for a practical use in an industrial environment where the ablation process has to be stable while achieving a high throughput.

A further improvement of the productivity can be accomplished by using pulse bursts instead of single pulse processing. The ablation rate could be raised by one order of magnitude while an energy that is ten times higher can be realized for the ablation process that supplies appropriate surface qualities.

The investigations of processing with bursts on grinded and ns-pretreated surfaces as well show that thermal heat accumulation can be used for smoothing the surface while ablating. Three ablation regimes were identified. Within the first regime no influence of heat accumulation can be observed. The resulting surface quality is strongly determined by the initial surface roughness. The second regime is of particular interest. Due to the number of pulses per burst and an adequate fluence heat accumulation forms a melt pool between 2 µm and 6 µm depth that smooths roughness peaks. Especially a precise ablation is possible if the following pulse burst impinges on a consolidated surface. As a result a ns-pretreated surface with an initial surface roughness of $R_a = 1.40$ µm could be improved to $R_a = 0.54$ µm during the ablation process with 4 PpB and a fluence of 2.3 J/cm² and 3.0 J/cm² respectively.

Ablation in the third regime is characterized by a melt dominated ablation similar to nanosecond processing. The final surface roughness can be predicted very well by the simulation model of the temperature distribution. The obtained melt pool depth correlates linear with the averaged surface roughness $R_z$.

The findings of the underlying examination help to increase the productivity of ultrashort pulsed micro ablation by achieving reasonable qualities. Focusing on productivity an ablation rate of more than 13 mm³/min at a surface roughness less than 1.7 µm can be achieved. Focusing on surface quality an ablation rate of 4 mm³/min at a surface roughness less than 0.6 µm can be accomplished regardless of the initial surface roughness. For the combination process of nanosecond and picosecond pulsed laser ablation the results promise a further improvement of the throughput that has to be shown in next examinations. Furthermore in following investigations the observed effects have to be proofed for a wider range of ns-pretreated surface qualities. The simulation model can support this investigations while its suitability will be reviewed at the same time.

**Acknowledgments and Appendixes**

This work is supported by the German Federal Ministry of Education and Research (BMBF) under the grant number 02P14A145 (eVerest). Furthermore we would like to acknowledge the support from the project partner Amphos for our experimental work in their application laboratory using the high power ultrafast laser system.

**References**

[1] A. Dunn, K. L. Wlodarczyk, J. V. Carstensen, E. B. Hansen, J. Gabzdyl, P. M. Harrison, J. D. Shephard, and D. P. Hand: Appl. Surf. Sci., 357, (2015) 2313.

[2] D. Braun, C. Greiner, J. Schneider, and P. Gumbsch: Trib. Inter., 77, (2014) 142.

[3] G. Ryk and I. Etsion: Wear, 261, (2006) 792.

[4] A. Dohrn and A. Gillner: Application Center. Laser Structuring for Tool and Mold Construction, <https://www.ilt.fraunhofer.de/content/dam/ilt/en/documents/product_and_services/laser_material_processing/B_Application_Center_Laser_Structuring_for_Tool_and_Mold_Construction_2015.pdf>.

[5] A. Brenner, F. Kurzidim, C. Fornaroli, and A. Gillner: JLA, 30, (2018) 32509.

[6] B. N. Chichkov, C. Momma, S. Nolte, F. Alvensleben, and A. Tünnermann: Appl. Phys. A, 63, (1996) 109.

[7] Y. Zhu, J. Fu, C. Zheng, and Z. Ji: Opt. & Laser Tech., 83, (2016) 21.

[8] K.-H. Leitz, B. Redlingshöfer, Y. Reg, A. Otto, and M. Schmidt: Phys. Proc., 12, (2011) 230.

[9] F. Bauer, A. Michalowski, T. Kiedrowski, and S. Nolte: Opt. Express, 23, (2015) 1035.

[10] R. Weber, T. Graf, P. Berger, V. Onuseit, M. Wiedenmann, C. Freitag, and A. Feuer: Opt. Express, 22, (2014) 11312.

[11] A. Y. Vorobyev and C. Guo: Appl. Phys. Lett., 86, (2005) 11916.

[12] A. Y. Vorobyev, V. M. Kuzmichev, N. G. Kokody, P. Kohns, J. Dai, and C. Guo: Appl. Phys. A, 82, (2006) 357.

[13] J.-T. Finger: Puls-zu-Puls-Wechselwirkungen beim Ultrakurzpuls-Laserabtrag mit hohen Repetitionsraten, 1. Auflage, (Apprimus, Aachen, 2017) p.40.

[14] B. Neuenschwander, T. Kramer, B. Lauer, and B. Jaeggi: Proc. SPIE, 9350, (2015) 93500U.

[15] G. Raciukaitis: JLMN, 4, (2009) 186.

[16] R. Le Harzic, D. Breitling, M. Weikert, S. Sommer, C. Föhl, S. Valette, C. Donnet, E. Audouard, and F. Dausinger: Appl. Surf. Sci., 249, (2005) 322.

[17] B. Jaeggi, B. Neuenschwander, M. Schmid, M. Muralt, J. Zuercher, and U. Hunziker: Phys. Proc., 12, (2011) 164.

[18] B. Neuenschwander, B. Jaeggi, M. Schmid, V. Rouffiange, and P.-E. Martin: Proc. SPIE, 8243, (2012) p. 824307.

[19] B. Jaeggi, B. Neuenschwander, S. Remund, and T. Kramer: Proc. SPIE, 10091, (2017) 100910J.

[20] B. Neuenschwander, B. Jaeggi, T. Kramer, and S. Remund: Proc. ICALEO, M301, San Diego, (2016) 1.

[21] S. Russ, R. Gebs, L. Bauer, U. Keller, T. Meyer, J. Roller, B. Führa, and B. Faisst: Proc. LiM, München, (2015) 161.

[22] J. Finger, B. Bornschlegel, M. Reininghaus, A. Dohrn, M. Nießen, A. Gillner, and R. Poprawe: Ad. Opt. Tech., 7, (2018) 145.

(Received: July 25, 2018, Accepted: March 31, 2019)